MTLA 34 (2024) 102062

Contents lists available at ScienceDirect

Materialia

journal homepage: www.elsevier.com/locate/mtla

Full Length Article

Liquid lithium corrosion of SiC/SiC composites

Junliang Liu [a,*], Harry Myers [a], Bradley Young [a], Alex Leide [b], James Wade-Zhu [b], Chris Grovenor [a], David E.J. Armstrong [a,*]

[a] Department of Materials, University of Oxford, 16 Parks Road, Oxford, OX1 3PH, United Kingdom
[b] United Kingdom Atomic Energy Authority, Culham Science Centre, Abingdon, Oxfordshire, OX14 3DB, United Kingdom

ARTICLE INFO

Keywords:
SiC/SiC
Liquid Metal Corrosion
Liquid Lithium
Tritium Breeding Blanket

ABSTRACT

Silicon carbide fibre reinforced silicon carbide matrix composite (SiC/SiC) is a key structural material for fusion reactors to allow high temperature operation of liquid lithium breeder blankets. This research investigated the corrosion behaviour of two SiC/SiC composites (using Tyranno SA3 and SA4 fibres) immersed in static liquid lithium at 600 °C for 100 h. Utilizing immersion tests and advanced microstructural analysis, the study reveals considerable corrosion in SiC/SiC composites, particularly in local areas enriched with residual carbon or oxygen. The interface carbon layer, while enhancing mechanical properties, induces preferential sites for corrosion cracking, diminishing the material's corrosion resistance. This study offers critical insights into the corrosive interaction between SiC/SiC composites and liquid lithium, highlighting the need for manufacturing process optimization and exploration of alternative interface layers, protective coatings, or avoiding contact between SiC/SiC and molten lithium in breeder blanket system.

Fusion energy represents a power source with immense potential for addressing some of humanity's most pressing energy challenges. Deuterium-tritium (D-T) fuel mix is currently viewed as the most viable option for achieving practical nuclear fusion energy, as it necessitates considerably lower temperatures and pressures in comparison to other fusion reactions. However, the large-scale implementation of D-T fuel mix would demand a substantial increase in the production and supply of tritium, a radioactive isotope that is not naturally abundant and has a half-life of only 12.3 years. To address this, researchers have proposed a variety of tritium breeding blanket concepts whereby the fusion neutrons interact with lithium (Li) to produce new tritium fuel. These blanket designs employ different combinations of structural materials, tritium breeding materials, and cooling materials. Among these, liquid lithium is considered one of the most promising tritium breeding materials for fusion demonstration power plants and commercial fusion reactors [1].

Compared to Li-ceramics, Li-Pb alloys, and molten-salt FLiBe (LiF and BeF2), liquid lithium offers a higher atomic density of Li atoms, allowing for a high tritium breeding ratio (TBR) and enabling 'tritium self-sufficiency' without the need for a neutron multiplier, like Be, in both Tokamak and Helical reactor systems [2]. However, the application of liquid lithium as a coolant or breeding material in fusion reactors presents considerable challenges in selecting appropriate materials due to its highly corrosive nature. Materials exposed to liquid lithium must not only resist liquid lithium corrosion but also endure the extreme conditions within reactors, such as high heat flux, temperature gradients, magnetic fields, radiation levels, and neutron flux, while preserving their mechanical properties over extended periods.

These challenges have spurred significant research interests into selecting materials capable of withstanding the corrosive environment of liquid lithium. SiC/SiC composite material is one of the most promising candidate materials in fusion reactor blankets due to its: low induced activity, low neutron cross-section, high dose irradiation resistance, high chemical stability, and heat resistance [3]. Previous studies have demonstrated that SiC exhibits good corrosion resistance to liquid Pb-17at%Li up to 1100 °C [4–6]. Literature on the compatibility of SiC/SiC composites with liquid lithium is scarce. Overall, however, the materials' performance has been reported to be significantly worse in comparison to Pb-Li alloys, associated with the higher thermodynamic stabilities of most Li compounds in liquid lithium relative to Pb-Li, and the lower solubility of O in Pb-Li [5,7,8]. Based on 450 °C corrosion tests in flowing liquid lithium for 315–617 h, Park et al. found that a hot pressed grade of monolithic SiC was compatible, while CVD and silicon-enriched SiC were heavily corroded [9]. They hypothesised that silicon, carbon, and oxygen impurities at grain boundaries react with lithium and cause failure of the material, although little further

* Corresponding authors.
E-mail addresses: junliang.liu@materials.ox.ac.uk (J. Liu), david.armstrong@materials.ox.ac.uk (D.E.J. Armstrong).

https://doi.org/10.1016/j.mtla.2024.102062
Received 15 October 2023; Accepted 11 March 2024
Available online 11 March 2024

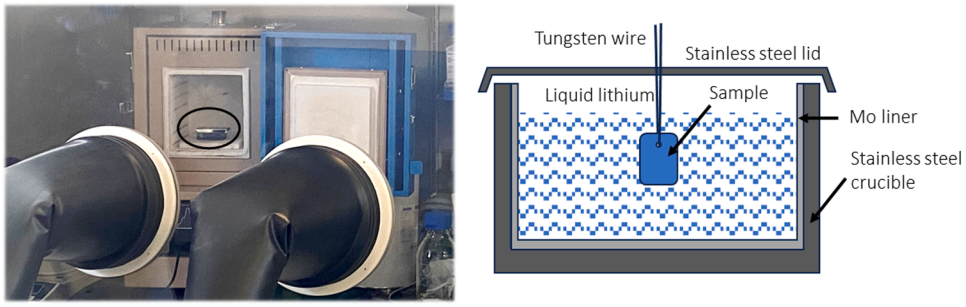

Fig. 1. The furnace inside a glovebox used for liquid lithium corrosion test and a schematic of the steel crucible with a Mo liner for immersing samples.

detail was provided. Static immersion of high purity CVD SiC in liquid lithium at 300 °C for 20 h showed insignificant change to the specimen, however little experimental detail is given [10] and the temperature is below the operational temperature of most breeder blankets designs. The majority of prior research has primarily reported on corrosion behaviour of SiC/SiC composites based on mass changes, optical microscopy or low-magnification electron microscopy characterisation [5, 9,10], which has led to a gap in the literature regarding high-resolution characterisation. Such detailed analysis is crucial to gain a mechanistic understanding of corrosion behaviour.

To better evaluate and understand the corrosion performance of SiC/SiC composite at elevated temperatures, we conducted static immersion tests in liquid lithium and employed Focused Ion Beam (FIB), Scanning Electron Microscope (SEM) and Energy-Dispersive X-ray Spectroscopy (EDX) characterisation techniques to provide insights into the key factors affecting its corrosion behaviour. Two "nuclear-grade" SiC/SiC composites that were manufactured using a propriety Chemical Vapor Infiltration (CVI) process were studied. The first materials, provided by General Atomics, San Diego, US as studied in [11], contains Tyranno SA3 fibres and the second provided by UKAEA, Culham, UK contains SA4 fibres. Both SA3 and SA4 are designated a "nuclear grade fibres", as they are described as stochiometric, however previous work has shown substantial free carbon in the core of SA3 fibres [11]. The SA4 fibres have been developed to further reduce this free carbon content [12]. Fibres were firstly coated with an interphase of ~100 nm of pyrolytic carbon (PyC). The matrix was subsequently deposited onto the coated fibres using the CVI method. During manufacturing, conditions were varied to favour infiltration and slow deposition in the early stages, with faster deposition to grow the material faster in later stages. This process was completed over several steps. The thin PyC coating around SiC fibres acts as a weak interface for the fibre to debond from the matrix and enable composite toughening mechanisms such as crack bridging and fibre pull-out to improve the mechanical properties [3].

Samples for corrosion tests were cut from near the centre of a large 25 cm x 25 cm x ~4 mm panel (SA4 Fibres) and from the centre of a 10 cm x 10 cm x 2 mm panel (SA3) into two ~ 1 cm x 1 cm squares using a slow speed diamond saw. They were then drilled with a 2 mm through-hole for hanging from a tungsten wire in the crucible. As depicted in Fig. 1, the corrosion tests were carried out in a stainless-steel crucible with a molybdenum (Mo) liner in an argon filled glove box. Mo is relatively inert when in contact with liquid lithium [13], and is selected as the liner material to avoid direct contact between the stainless-steel crucible and the liquid lithium. The lithium was initially melted in the liners, and the samples were then introduced into the container and partially immersed in the liquid lithium. The corrosion tests were conducted at a temperature of 600 °C for a duration of 100 h inside a furnace inside the argon filled glove box. The lithium was purchased from Alfa Aesar® with purity of >99.9 %, and the argon purity was < 0.1 ppm oxygen and < 0.1 ppm H_2O. After corrosion, the samples were extracted from the liquid lithium and cooled inside the glove box. After cooling, the samples were transferred into a solution of 95 % ethanol, 5 % water, to remove the residual lithium solidified on the surface. The samples were weighed before and after corrosion. For the SA4 based sample ~ 20 % mass loss after corrosion was observed. The SA3 sample could not be accurately weighed due to its fragile nature after corrosion and was directly mounted for FIB/SEM. FIB-SEM characterisation was performed on both as-received and corroded samples to reveal the microstructural changes on a Thermo Scientific Helios G4 system equipped with an Oxford Instrument EDX detector.

The typical microstructure of the as-received SA3 and SA4 based SiC/SiC composites is illustrated in Fig. 2(a-1, a-2, b-1 and b-2). It consists of SiC fibres, the SiC matrix, and residual porosity. Surrounding each fibre, multiple rings can be observed, as depicted in Fig. 2 (b-2). The innermost ring corresponds to the carbon interlayers coated on the SiC fibre prior to CVI. Three additional rings with lighter contrast compared to the carbon interlayers can be seen in the SA4 samples, and EDX analysis indicates that these rings are oxygen-enriched as shown in Fig. 3(a), likely formed during multiple CVI runs. Another notable feature is the non-uniform contrast within the fibre, with a darker centre and brighter periphery. EDX elemental analysis in Fig. 3 reveals that these dark central regions within the fibre are rich in carbon and depleted of silicon. This suggests that they are likely precipitates of excess carbon. This is in agreement with previous work on SA3 fibres showing a similar carbon enrichment [11]. These microstructural observations are known to influence the corrosion performance and will be further discussed.

Fig. 2(a-3, a-4, b-3 and b-4) shows the FIB-SEM comparison of corrosion in the SA3 and SA4 fibres, specifically in sub-surface regions attacked by lithium. While both types of fibres have clearly been attacked and show porosity, the damage is significantly more severe in the SA3 fibre. The fibre becomes nanostructured with a central hole at the location of highest carbon content. In the SA4 fibres the central hole is present but there is significantly less damage towards the fibre edge. This is due to the reduced carbon content in SA4 fibres. Fig. 2(b-3) shows the first tows of SiC fibres beneath the thick outer CVD coating of the SA4 sample. This CVD SiC coating layer exhibits the formation of lateral, micron-scale cracks which appear to be aligned to the circumference of the fibres, similar to the oxidation rings shown in Fig. 2 (b-2). Additional circumferential cracks can be observed through the SEM in Fig. 2(b-4) which are corresponding to the carbon interphase and the oxygen-rich rings as shown by the EDX linescans in Fig. 3.

It needs to be noted that the FIB-SEM cross-sectional characterisation only provides information at shallow depths near the corrosion surface. To further investigate the corrosion behaviour deeper in to the bulk of the sample, the corroded SA4 specimen was mounted in Bakelite, cross-sectioned with a slow speed diamond saw, and subjected to mechanical polishing, revealing a cross-section which includes material submerged in lithium and material which was above the surface of the molten lithium during corrosion. SEM imaging from the polished cross-sectional surface of the submerged side is presented in Fig. 4. Even at this depth into the sample bulk (~0.5 cm from sample edges), extensive corrosion is evident, with central regions within most of the fibres preferentially attacked. Another interesting feature is that a series of cracks are formed surrounding the fibres, aligning well with the locations of the dark rings

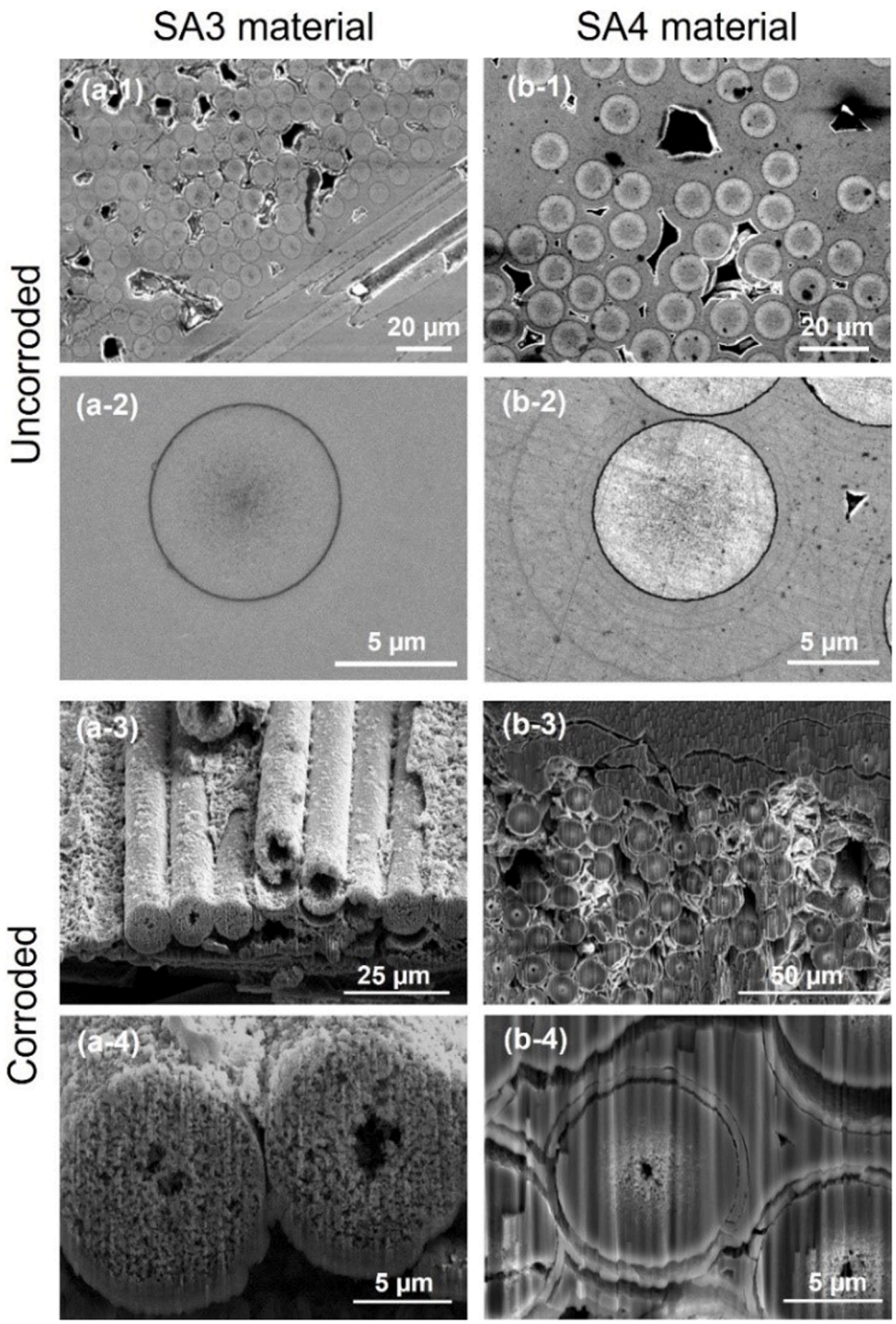

Fig. 2. Secondary electron SEM images of SA3 and SA4 materials, (a-1, a-2, b-1 and b-2) before corrosion, (a-3, a-4 b-3 and b-4) after corrosion.

in the as-received samples depicted in Fig. 2(b-2). The observation of corrosion cracks together with the EDX results in Figs. 2–4 could lead to the conclusion that the carbon and oxygen enriched regions (the fibre centres, the carbon interlayers, and the oxygen-enriched interface regions) were preferentially attacked during liquid lithium corrosion, agreeing with the hypothesis in [9].

At the same sample depth, significantly different microstructures of corroded fibres and matrix are observed in Fig. 4(b), (c) and (d) near to each other in the sample. The fibres and SiC matrix generally demonstrate three typical corroded microstructures:

(1) Both the fibre centres and the surrounding rings were heavily corroded, forming cracks/holes, Fig. 4(b).
(2) the fibre centres were corroded while the surrounding CVI SiC layers exhibited less corrosion, Fig. 4(c).
(3) some fibre centres showed less corrosion, whereas the surrounding rings were heavily corroded and cracked, Fig. 4(d).

These corroded microstructures firstly imply that channels may be formed, facilitating the easy penetration of liquid lithium into the inner regions of the samples, potentially through pre-existing porosity and corrosion-induced cracks. Secondly, the variations in the extent of corrosion in different fibres implies locally variations in Li exposure,

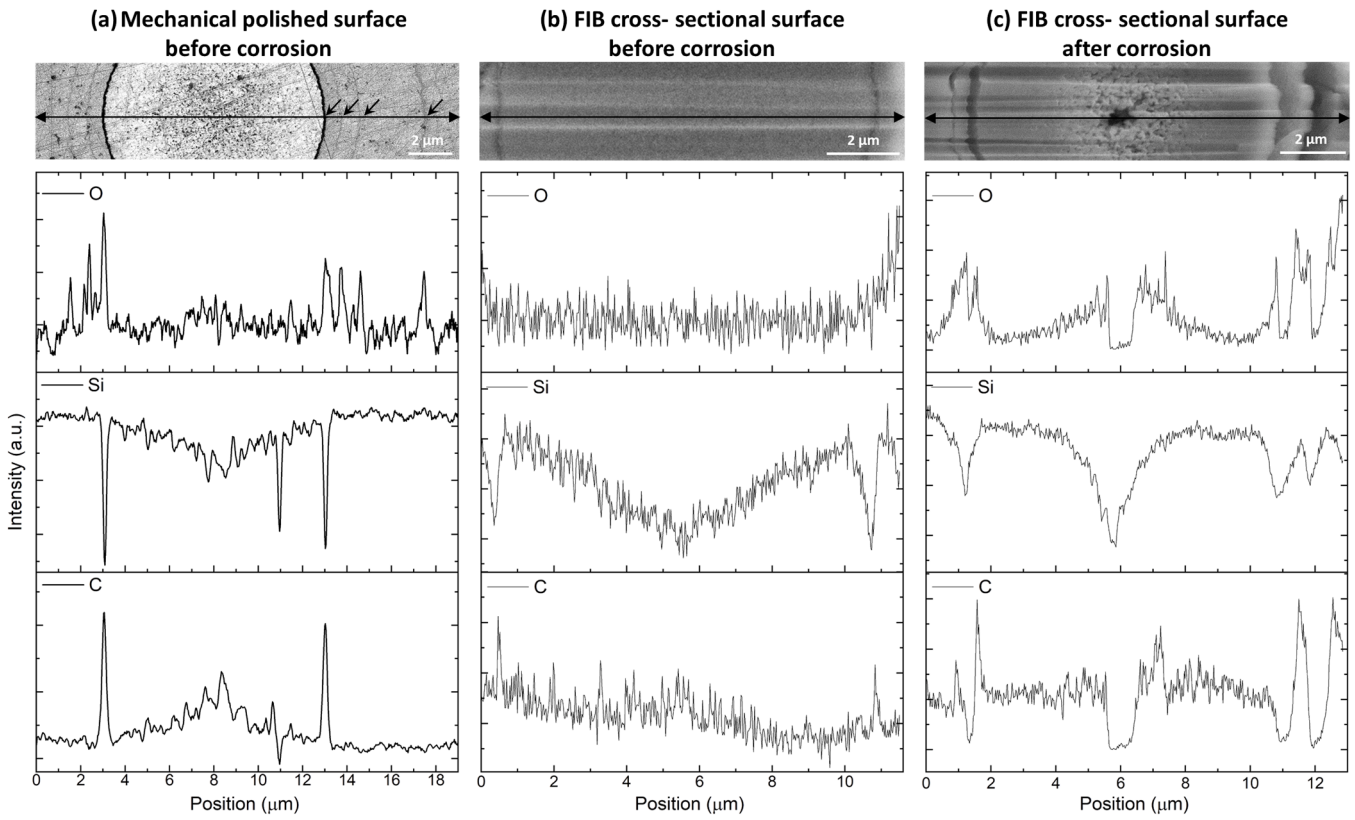

Fig. 3. SEM and EDX linescans from SA4 samples: (a) mechanically polished surface before corrosion, (b) FIB cross-sectional surface before corrosion, and (c) FIB cross-sectional surface after corrosion. The carbon interphase and the oxygen-rich rings are highlighted by arrows in the SEM image in (a).

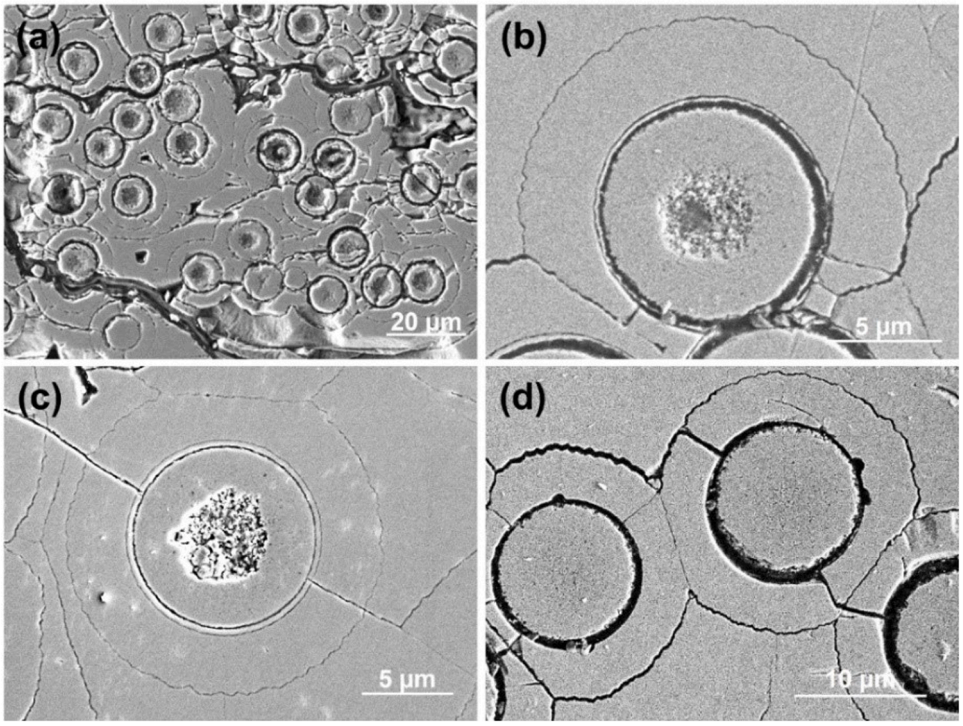

Fig. 4. Secondary electron SEM images showing the morphology of SiC/SiC composite at the mechanical polished cross-section of the test coupon, away from the coupon surfaces. In (a) there is a variation of the extent of fibre corrosion. (b) and (c) show corrosion features similar to the FIB cross-sections near the surface. (d) shows less corroded fibres. Radial cracks are visible in (b) - (d).

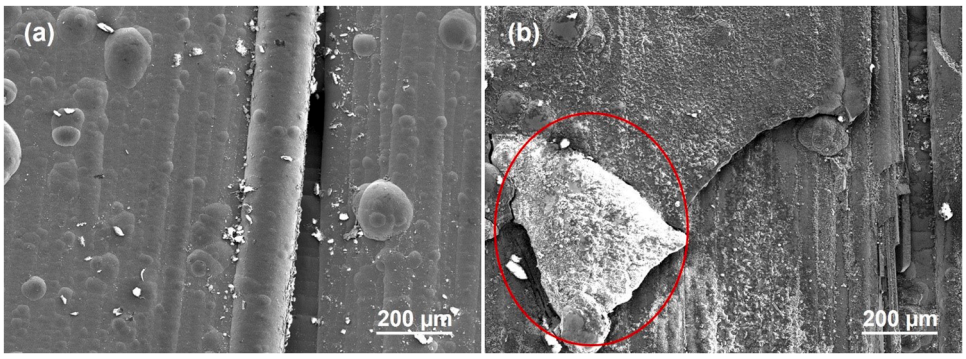

Fig. 5. Typical secondary electron SEM images showing unpolished surface microstructure of (a) as-received and (b) corroded samples. The SiC flake in brighter contrast in (b) is presumably ready to flake off.

which is a result of factors effecting the proximity of Li with C and O as well as availability/quantity of free C and O. The possible factors includes the local thickness of C interphase, oxide scale thickness on fibres and the distributions of radial cracks in matrix.

Considering the small scale of the carbon interphase and oxygen-rich rings which have been corroded, this does not appear to account for the approximately 20 % mass loss of the specimens. Mass loss is probably associated with the exfoliation of SiC layers caused by corrosion of the carbon interface and oxygen-rich rings which combined with cracking led to sections of coating flaking off, Fig. 5.

Unlike in the Pb-Li at eutectic composition (17 %Li), Li_2C_2 is thermodynamically stable in liquid lithium [7], which provides a key corrosion pathway for SiC in Li. In other corrosive systems, such as hydrothermal corrosion in light water reactor conditions, or oxidation in molten salt corrosion in FLiNaK or FLiBe cooled reactors, off-stoichiometric features in SiC tend to be attacked, such as grain boundaries, residual phases or impurities [14–17]. The fact that we see severe corrosion of the fibre core would support the idea that carbon is the primary reactant as the SiC in those regions are likely to be off-stoichiometry and carbon-rich.

It must be noted that all SEM observations were conducted after removing the lithium adhered to the samples. Consequently, if any compound formation occurred and if such compounds were eliminated by the cleaning solution (comprising 95% ethanol and 5% water), we would not be able to characterise them in this context. According to phase diagrams [18,19], both silicon and carbon possess substantial solubility in liquid lithium at elevated temperatures, and they can form a variety of compounds. It is, therefore, essential to develop a method that allows the characterisation of the corroded sample surface without removing the surface lithium. In this scenario, the microstructure of any compound(s) formed at the lithium/sample interface could be characterised. This approach would contribute significantly to a deeper understanding of the corrosion mechanisms of SiC in liquid lithium.

In summary, the SiC/SiC composite demonstrates significant corrosion after a 100-hour immersion in static liquid lithium at 600 °C. The formation of cracks and pores is particularly prominent in areas known to be enriched with residual carbon or oxygen such as the central regions of the fibres, the circumference of the fibres, and the halo-rings between layers of CVI SiC. The more stoichiometric CVI SiC layers appear to be resistant to lithium corrosion in the current conditions, however, the composition and Si:C ratio is predicted to change due to transmutation during operation in a fusion environment which may lead to enhanced corrosion over time [20]. While the interface carbon layer has been shown to enhance mechanical properties and radiation resistance [3], it is seen to compromise resistance to liquid lithium corrosion by providing preferred sites for corrosion cracking. During the corrosion process, pores originating from manufacturing interconnect with the corrosion-induced cracks. This network of cracks may further facilitate the easy penetration of liquid lithium into the deeper regions of the samples. These findings underscore the need for optimization in the manufacturing process of SiC/SiC composites, specifically to reduce the enrichment of these potentially detrimental elements. Furthermore, it highlights the need of investigating alternative interface layers, which can maintain the mechanical properties under irradiation while also provide corrosion resistance to liquid lithium. Aerospace-grade BN is ruled out due to helium production and activation issues. There has been some progress on interphaseless composites and the use of other carbon free materials for the interphase, such as yttrium disilicate fibre coatings [21,22]. However, more work is needed to test these alternatives, with respect to both their mechanical performance and corrosion resistance.

Declaration of competing interest

The authors declare that they have no known competing financial interests or personal relationships that could have appeared to influence the work reported in this paper.

Acknowledgement

The authors would like to acknowledge Dr Christian Deck for providing SiC/SiC samples as part of the study. J.L., H.M, C.R.M.G. and D.E.J.A. would acknowledge funding support from the Royce Institute. A.J.L. was supported by the Royal Academy of Engineering under the Research Fellowship programme. The authors acknowledge the use of characterisation facilities within the David Cockayne Centre for Electron Microscopy (DCCEM), Department of Materials, University of Oxford. This work was supported by funding from the Engineering and Physical Sciences Research Council (EPSRC) [EP/W006839/1].

References

[1] A. de Castro, C. Moynihan, S. Stemmley, M. Szott, D.N. Ruzic, Lithium, a path to make fusion energy affordable, Phys. Plasmas. 28 (2021) 50901, https://doi.org/10.1063/5.0042437.
[2] S. Konishi, M. Enoeda, M. Nakamichi, T. Hoshino, A. Ying, S. Sharafat, S. Smolentsev, Functional materials for breeding blankets—Status and developments, Nucl. Fusion. 57 (2017) 92014, https://doi.org/10.1088/1741-4326/aa7e4e.
[3] T. Noda, Advanced SiC-SiC composites for nuclear application, Handb. Adv. Ceram. Compos. Defense, Secur. Aerosp. Energy Appl. (2020) 641–666.
[4] B.A. Pint, J.L. Moser, P.F. Tortorelli, Investigation of Pb–Li compatibility issues for the dual coolant blanket concept, J. Nucl. Mater. 367–370 (2007) 1150–1154, https://doi.org/10.1016/J.JNUCMAT.2007.03.206.
[5] T. Yoneoka, S. Tanaka, T. Terai, Compatibility of SiC/SiC composite materials with molten lithium metal and Li16-Pb84 eutectic alloy, Mater. Trans. 42 (2001) 1019–1023.
[6] F. Barbier, P. Deloffre, A. Terlain, Compatibility of materials for fusion reactors with Pb–17Li, J. Nucl. Mater. 307–311 (2002) 1351–1354, https://doi.org/10.1016/S0022-3115(02)00987-X.
[7] P. Hubberstey, Pb-17Li and lithium: a thermodynamic rationalisation of their radically different chemistry, J. Nucl. Mater. 247 (1997) 208–214, https://doi.org/10.1016/S0022-3115(97)00071-8.

[8] P. Hubberstey, T. Sample, Thermodynamics of the interactions between liquid breeders and ceramic coating materials, J. Nucl. Mater. 248 (1997) 140–146, https://doi.org/10.1016/S0022-3115(97)00204-3.
[9] J.H. Park, T. Domenico, G. Dragel, R. Clark, Development of electrical insulator coatings for fusion power applications, Fusion Eng. Des. 27 (1995) 682–695, https://doi.org/10.1016/0920-3796(95)90184-1.
[10] W. Lu, J. Wang, W. Pu, K. Li, W. Wang, S. He, D. Chu, J. Yang, Y. Zhu, Corrosion resistance of ceramic candidates for tritium permeation barriers exposed to molten lithium, Corros. Sci. 160 (2019) 108172, https://doi.org/10.1016/j.corsci.2019.108172.
[11] Y. Zayachuk, P. Karamched, C. Deck, P. Hosemann, D.E.J. Armstrong, Linking microstructure and local mechanical properties in SiC-SiC fiber composite using micromechanical testing, Acta Mater 168 (2019) 178–189, https://doi.org/10.1016/J.ACTAMAT.2019.02.001.
[12] J. Braun, C. Sauder, Mechanical behavior of SiC/SiC composites reinforced with new Tyranno SA4 fibers: effect of interphase thickness and comparison with Tyranno SA3 and Hi-Nicalon S reinforced composites, J. Nucl. Mater. 558 (2022) 153367, https://doi.org/10.1016/J.JNUCMAT.2021.153367.
[13] X. Meng, G. Zuo, Z. Sun, W. Xu, M. Huang, C. Xu, Y. Qian, W. Hu, J. Hu, H. Deng, Compatibility of Molybdenum, Tungsten, and 304 Stainless Steel in Static Liquid Lithium Under High Vacuum, Plasma Phys. Reports 44 (2018) 671–677, https://doi.org/10.1134/S1063780X18070036.
[14] X. Xie, B. Liu, Y. Guo, R. Liu, X. Zhao, N. Ni, F. Guo, P. Xiao, Effect of hydrothermal corrosion on the fracture strength of SiC layer in tristructural-isotropic fuel particles, J. Am. Ceram. Soc. 102 (2019) 5555–5564, https://doi.org/10.1111/jace.16369.
[15] C. Liu, J. Xi, I. Szlufarska, Sensitivity of SiC Grain Boundaries to Oxidation, J. Phys. Chem. C. 123 (2019) 11546–11554, https://doi.org/10.1021/acs.jpcc.9b00068.
[16] P.J. Doyle, S. Zinkle, S.S. Raiman, Hydrothermal corrosion behavior of CVD SiC in high temperature water, J. Nucl. Mater. 539 (2020) 152241, https://doi.org/10.1016/j.jnucmat.2020.152241.
[17] J.J. Lee, S.S. Raiman, Y. Katoh, T. Koyanagi, C.I. Contescu, X. Hu, Y. Yang, Chemical compatibility of silicon carbide in molten fluoride salts for the fluoride salt-cooled high temperature reactor, J. Nucl. Mater. 524 (2019) 119–134, https://doi.org/10.1016/j.jnucmat.2019.07.001.
[18] H. Okamoto, The C-Li (Carbon-Lithium) system, Bull. Alloy Phase Diagrams. 10 (1989) 69–72, https://doi.org/10.1007/BF02882178.
[19] H. Okamoto, Li-Si (Lithium-Silicon), J. Phase Equilibria Diffus. 30 (2009) 118–119, https://doi.org/10.1007/s11669-008-9431-8.
[20] M.E. Sawan, Y. Katoh, L.L. Snead, Transmutation of silicon carbide in fusion nuclear environment, J. Nucl. Mater. 442 (2013) S370–S375, https://doi.org/10.1016/j.jnucmat.2012.11.018.
[21] E.E. Boakye, T.S. Key, P. Mogilevsky, S.J. Opeka, R. Corns, R.S. Hay, M.K. Cinibulk, SiC/SiC mini-composites with yttrium disilicate fiber coatings: oxidation in steam, J. Eur. Ceram. Soc. 41 (2021) 3132–3140, https://doi.org/10.1016/j.jeurceramsoc.2020.09.033.
[22] K. Shimoda, T. Hinoki, Y.H. Park, Development of non-brittle fracture in SiCf/SiC composites without a fiber/matrix interface due to the porous structure of the matrix, Compos. Part A Appl. Sci. Manuf. 115 (2018) 397–404, https://doi.org/10.1016/j.compositesa.2018.10.005.